Carbon 126 (2018) 544–551

Contents lists available at ScienceDirect

Carbon

journal homepage: www.elsevier.com/locate/carbon

# Terahertz spectroscopy of charge transport in films of pristine and doped single-wall carbon nanotubes

B.P. Gorshunov [a, **], E.S. Zhukova [a, *], Ju.S. Starovatykh [a], M.A. Belyanchikov [a], A.K. Grebenko [a], A.V. Bubis [a], V.I. Tsebro [b], A.A. Tonkikh [c], D.V. Rybkovskiy [c], A.G. Nasibulin [d, e, f], E.I. Kauppinen [e], E.D. Obraztsova [c]

[a] Moscow Institute of Physics and Technology, Dolgoprudnyi, Moscow Region, 141700 Russia
[b] P.N. Lebedev Physical Institute, RAS, 53 Leninskyi Prospect, 119991 Moscow, Russia
[c] A.M. Prokhorov General Physics Institute, RAS, Moscow, 119991 Russia
[d] Skolkovo Institute of Science and Technology, Nobel str. 3, 143026, Moscow, Russia
[e] Department of Applied Physics, Aalto University, School of Science, P.O. Box 15100, FI-00076, Espoo, Finland
[f] National University of Science and Technology "MISIS", Leninskyi Prospect, 4, Moscow, 119049, Russia

ARTICLE INFO

*Article history:*
Received 24 July 2017
Received in revised form
12 October 2017
Accepted 21 October 2017
Available online 23 October 2017

ABSTRACT

Electrical transport mechanisms of 2D carbon nanotube networks are presently under intensive studies. The related experimental data are ambiguous and controversial. We report on terahertz-infrared spectra of optical conductivity and dielectric permittivity of thin transparent films composed of pristine and CuCl- or iodine-doped single-walled carbon nanotubes (SWCNTs) measured in the frequency range from 7 to 25 000 $cm^{-1}$ and at temperatures from 5 to 300 K. Controversially to the existing results, we have not observed a clear signature of the so-called terahertz conductivity peak. Instead, a typical metallic-like frequency- and temperature-dependent behavior of the conductivity and permittivity has been discovered. It was attributed to the high quality interconnected SWCNT network providing the almost free pathways for charge carriers. Applying Drude conductivity model, we have determined the temperature and doping dependences of effective parameters of the carriers in the films: plasma frequency, scattering rate, mobility, mean-free path. The obtained results demonstrate a great potential of the material in the field of electromagnetic applications at frequencies up to few terahertz.



## 1. Introduction

Due to their unique physical and chemical properties, single-walled carbon nanotubes (SWCNTs) attract a lot of attention from both fundamental and application points of view [1–4]. The diversity of these properties is determined by their one-dimensional geometry and by the way of their rolling up [5]. Since every atom in a SWCNT is located on the surface the properties of this material strongly depend on the presence of foreign atoms/molecules as well as contacts with other tubes and substrates. Moreover, the properties of the tubes can be tuned by insertion of various compounds inside the tubes.

Along with an extensive activity in the field of exploring properties of individual tubes, two-dimensional layers or films of the SWCNTs composed of large number of randomly distributed or aligned nanotubes attract a considerable interest [6,7]. Such nanotube networks are appropriate for designing novel micro- and macro-electronic devices and elements, like transparent, flexible and stretchable electrical conductors, coatings and screens, electromagnetic shields, chemical and biological sensors, polarizers, antennas and many others. Implementation of SWCNT films for such applications strongly motivates studies of their electrical and optical characteristics that can significantly differ from those of separate SWCNTs due to the length and diameter distributions, presence of both metallic and semiconductor types, and intertube interaction. In this respect, optical spectroscopy in the energy range of 1 eV is widely used to study electronic transitions related to the van Hove singularities in the SWCNT density of states. However, the central interest for the practical purposes is the electronic states

* Corresponding author.
** Corresponding author.
*E-mail addresses:* bpgorshunov@gmail.com (B.P. Gorshunov), zhukova.es@mipt.ru (E.S. Zhukova).

https://doi.org/10.1016/j.carbon.2017.10.072
0008-6223/

close to the Fermi level, since they determine the dc charge transport and low-energy electrodynamics of SWCNTs in a separate state as well as in the thin film conformation. Corresponding experimental investigations in the infrared, far-infrared (FIR) and terahertz (THz) ranges sometimes report controversial results obtained by various groups. One of the discrepancies concerns the so-called terahertz conductivity peak that is observed in the conductivity or absorbance spectra at the frequencies that range from about 30 THz [8] to 0.4 THz [9]. Two different interpretations for the origin of the peak have been recently proposed. The first one considered the small energy gap in the density of states caused by the finite curvature of the quasi-metallic tubes [10–14], whereas the second interpretation is based on the plasmonic oscillations of charge carriers within the finite-length of the SWCNTs [8,15–19]. The lack of consensus regarding the nature of the peak together with the inconsistency in the available experimental data hinder the revealing of the microscopic mechanisms of the dc charge transport and low-frequency dynamics of charge carriers in these objects.

Here, we have performed a comprehensive broad-band spectroscopic investigation of high-quality pristine and doped (iodine, CuCl) SWCNT films. By measuring the terahertz to infrared spectra of conductivity and dielectric permittivity of the films in the temperature range from 5 to 300 K and analyzing the spectra together with the dc conductivity data, we show that the THz conductivity peak is transformed in our samples into a Drude band of 60–80 $cm^{-1}$ width revealing the metallic response due to the quasi-free charge carriers. As a result, we were able to determine the effective parameters of the charge carriers in the networks: mobility, concentration, mean-free path, collision time, plasma frequency. In addition to the fundamental importance of our work, we have also demonstrated that the investigated SWCNT films can be utilized for electromagnetic shielding applications.

## 2. Experimental details

An aerosol CVD technique was used for the synthesis of SWCNTs, as described in Refs. [20,21]. Briefly, the SWCNTs were synthesized in the gas phase by ferrocene vapor decomposition in the atmosphere of carbon monoxide and deposited on a nitrocellulose filter in the form of individual and small diameter bundles. The SWCNT film can be easily transferred on practically any other substrate [22] or utilized in a free-standing form [7]. To dope the SWCNTs, they were subjected to a special treatment in vapors of iodine or CuCl that resulted in filling the nanotubes with the dopant molecules and in obtaining the doped SWCNT films without any change of the SWCNT network morphology [23–25]. The average diameter of the SWCNTs, 2 nm, was determined according to the electronic transitions energies dependence on the nanotube diameter [26–28]. The thicknesses of the SWCNT films were estimated by a scanning electron microscopy.

To characterize the pristine and doped SWCNT films we performed Kelvin-probe measurements with the NanoScanTech Certus Standart V in a dual-pass regime. The Micromach N18 cantilever with Au/Ti coverage was used. The films were placed on the surface of silicon wafers and densified with isopropanol. Fig. 1a shows a typical topography of the pristine film, whose potential relief (Fig. 1b) shows that there are rather long paths with nearly uniform potential that is not markedly influenced by the tubes intersections or by any kind of the defects inside the tubes. The pattern, of course, does not reproduce the potential relief that can be felt by the carriers and that is too shallow to be detected by the equipment due to its limited spatial resolution and sensitivity. In order to prove in more details the homogeneity of the potential along the separate SWCNTs, we performed Kelvin-probe measurements on the single carbon nanotubes with lithographically fabricated Au/Ti contacts, as shown in the topography image in Fig. 1c. The potential variation along the tube (Fig. 1d) is very smooth and uniform indicating an intrinsic character of the charge carriers' scattering and the absence of any defects that could lead to abrupt drops of the potential. We were able to detect such kind of “external” defects, but their emergence was very rare. An example is shown in Fig. 1f where the sharp changes of the potential caused by internal strains or some other faults are not distinctly visualized on the topography of the tube (Fig. 1e). We thus conclude that the charge carriers can nearly freely travel not only through a separate tube but also over much longer distances up to several micrometers (see Fig. 1a and b). Clearly, on their way they experience scattering processes due to phonons, tunnel barriers at the tubes intersections, defects/impurities, as discussed below.

High quality of SWCNTs composing our films is also demonstrated by Fig. 2 where an example of Raman spectrum taken on one of the studied samples is presented. Three groups of modes are seen in the spectrum: the low-frequency radial breathing modes (RBM), the disorder-induced modes (D-band) and the tangential modes (G-band). The intensity of the D-band modes (around 1322 $cm^{-1}$) is negligible small; it is more than 200 times lower than the intensity of the G-band.

All optical measurements were performed with free-standing films transferred from the nitrocellulose filters to a metallic ring with a clear aperture of 8 mm. At terahertz frequencies, from $\nu \approx 7$ to 60 $cm^{-1}$, the spectra of real and imaginary parts of complex conductivity $\sigma^*(\nu) = \sigma_1(\nu)+i\sigma_2(\nu)$ and dielectric permittivity $\varepsilon^*(\nu) = \varepsilon'(\nu)+i\varepsilon''(\nu)$ were registered with the TeraView time-domain spectrometer and the quasioptical monochromatic spectrometer based on backward-wave oscillators as sources of coherent THz-subTHz radiation [29]. In the infrared range, up to 25 000 $cm^{-1}$, the spectra of transmission coefficients of the SWCNT samples were measured using the Fourier-transform spectrometer Vertex 80 V. As a result of joint analysis of the THz and IR data the spectra of broad-band conductivity and permittivity of the samples have been provided. The home-made optical cryostats were used to examine the materials in the temperature interval from 5 to 300 K.

## 3. Results and discussion

Fig. 3a shows the measured room-temperature transmission coefficient spectra of the three samples of pristine, CuCl- and iodine-doped ≈100 nm thick SWCNT films. At frequencies from 3000 to 25 000 $cm^{-1}$, the characteristic local minima are seen. They correspond to the well-known electronic transitions due to van Hove singularities in the density of states. The rest of our paper will be devoted to the low-frequency data, namely to the IR and THz ones. Below 1000 $cm^{-1}$, a pronounced decrease of the transmissivity is observed that testifies the enhanced absorption, which is more pronounced in the doped films (cf. with the THz $\sigma_1$ and $\varepsilon''$ spectra displayed in Fig. 3b and c). The physical origin of this absorption is one of the most important issues discussed in our paper. It will be considered here on the basis of broad-band spectra of conductivity and dielectric permittivity obtained from the spectral analysis of the IR transmission coefficient spectra together with the directly measured THz $\sigma_1$, $\varepsilon'$ and $\varepsilon''$ spectra and with the dc conductivity values taken from our paper [30]. First of all, we state that the observed THz absorption cannot be caused by any resonance-like absorption associated with either the interband transition or plasmonic excitation mentioned above. This is so already for the reason that in such case the dc conductivity values, $\sigma_{dc}$, would be significantly smaller than the corresponding values of the THz conductivity (dots in Fig. 3b) that is, however, not the case: the $\sigma_{dc}$ values measured in Ref. [30] vary from ≈700 $\Omega^{-1}cm^{-1}$ (pristine) to

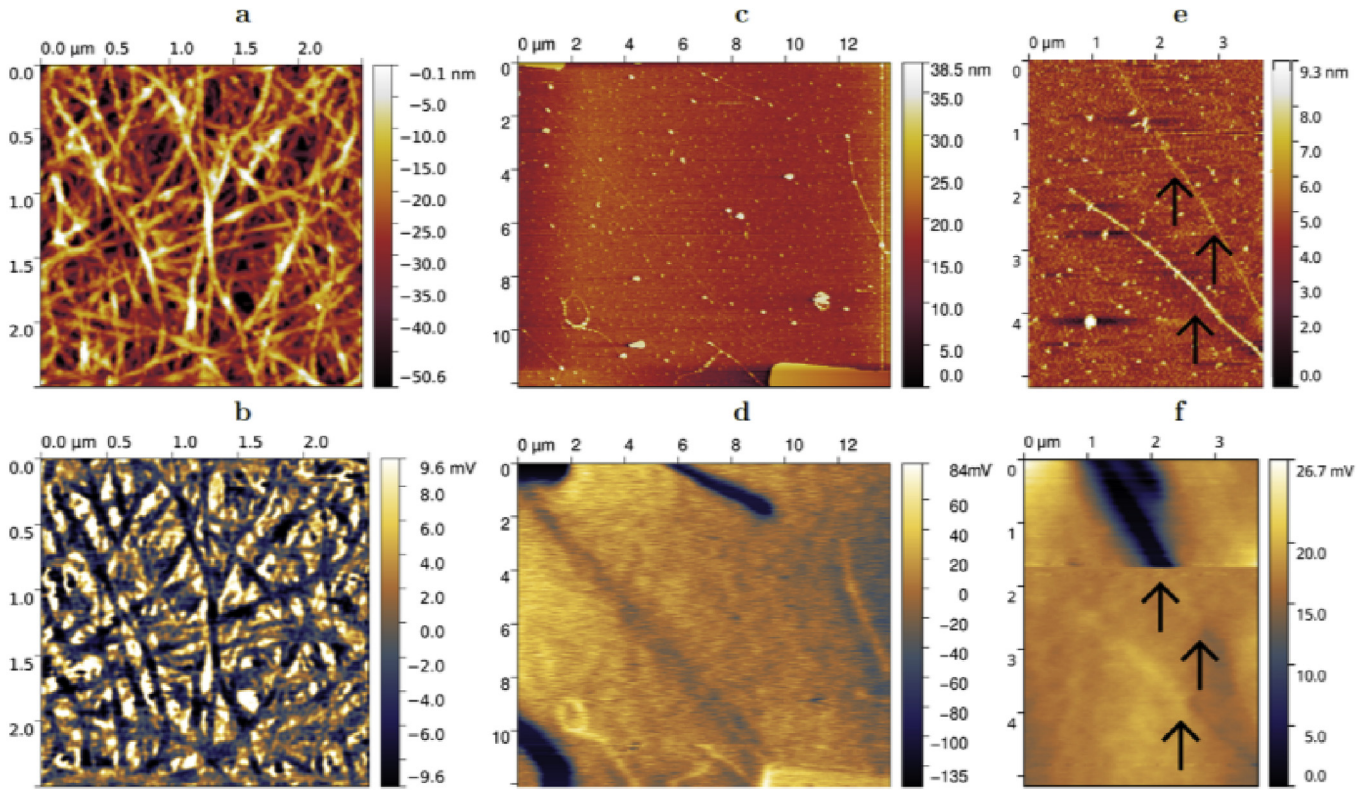


**Fig. 1.** Kelvin-probe force microscopy data obtained on pristine and doped SWCNT films. (a). Topography image of the pristine SWCNT film. False color bar on the right side indicates the penetration depth of the microscope tip. (b). Potential map of the same film. (c). Topography image of separate SWCNT with 2 contacts. (d). corresponding work-function map. The top contact is grounded and the bottom one is under approximately 200 mV. (e). Topography of the SWCNT with defects that are not visible in the morphology, but clearly seen on work-function map shown in (f). Defects cause potential drop and are indicated by black arrows. (A colour version of this figure can be viewed online.)

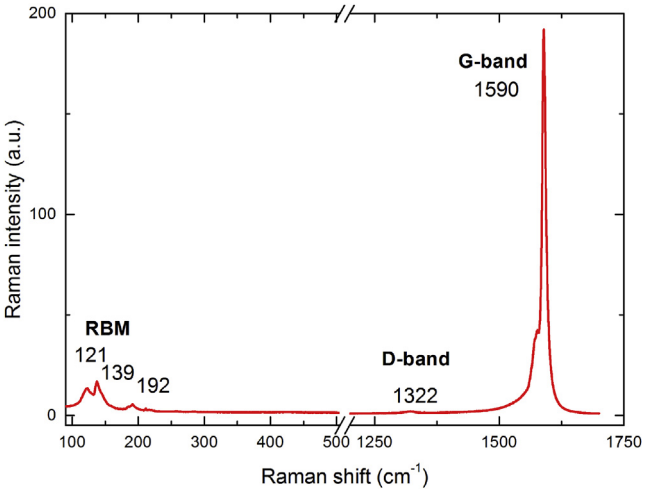


**Fig. 2.** Raman spectrum of a pristine film of single-wall carbon nanotubes, synthesized by aerosol method [20]. Indicated are radial breathing modes (RBM), the disorder-induced modes (D-band) and the tangential modes (G-band). (A colour version of this figure can be viewed online.)

$\approx$1700 - 2000 $\Omega^{-1}$cm$^{-1}$ (doped). Below we prove that the only way to account for the observed spectral behaviors of the THz conductivity and permittivity (Fig. 3b,c,d), together with the THz-IR transmission coefficient spectra (Fig. 3a), is to associate their origin with the response of delocalized charge carriers. We note that signatures of the free-carrier type ac response in SWCNT films were also found earlier in Refs. [31,32].

The spectral response of free charge carriers is usually described within the Drude conductivity model, where the frequency-dependent conductivity and permittivity are given as [33,34]:

$$\sigma^*(\nu) = \sigma_1(\nu) + i\sigma_2(\nu) = \frac{\sigma_{dc}\gamma^2}{\gamma^2+\nu^2} + i\frac{\sigma_{dc}\nu\gamma}{\gamma^2+\nu^2}, \quad (1)$$

$$\varepsilon^*(\nu) = \varepsilon'(\nu) + i\varepsilon''(\nu) = \varepsilon_0 - \frac{2\sigma_{dc}\gamma}{\gamma^2+\nu^2} + i\frac{2\sigma_{dc}\gamma^2}{\nu(\gamma^2+\nu^2)}, \quad (2)$$

where $\sigma_{dc} = \frac{\nu_{pl}^2}{2\gamma} = ne\mu = \frac{ne^2\tau}{m^*} = \frac{ne^2}{2\pi m^*\gamma}$is the dc conductivity, $\gamma$ is the charge-carrier scattering rate, $\nu_{pl}$ is the plasma frequency, $n$ is the concentration of charges, $e$ is the elementary charge, $\mu$ is the charge mobility, $\tau$ is the collision time, $m^*$ is the effective mass and $\varepsilon_0$ is the high-frequency contribution to the permittivity.

According to (1, 2), in case of low frequencies, $\nu \ll \gamma$, the real part of the conductivity does not strongly depend on the frequency, $\sigma_1 \approx$const, with the imaginary permittivity being inversely proportional to the frequency, $\varepsilon'' = 2\sigma_1/\nu \propto 1/\nu$ (dashed line in Fig. 3c). $\sigma_1(\nu)$ falls down around the scattering rate frequency $\gamma$, where at $\nu = \gamma$ the imaginary part $\sigma_2$ of the conductivity acquires its maximum value dashed lines in Fig. 3b). In addition, in the low-frequency limit, $\nu \ll \gamma$, the real permittivity $\varepsilon'$ acquires negative values. These typical signatures of metallic spectral behavior are broadly observed in various conductors [33] and they are clearly seen in the THz spectra of the doped SWCNT films shown in Fig. 3b,c,d. Metallic character of the THz spectra of the doped films is also confirmed by their temperature evolution, as shown in Fig. 4: while cooling, the THz conductivity grows up and the THz permittivity $\varepsilon'$ goes down, more to the negative values. As to the

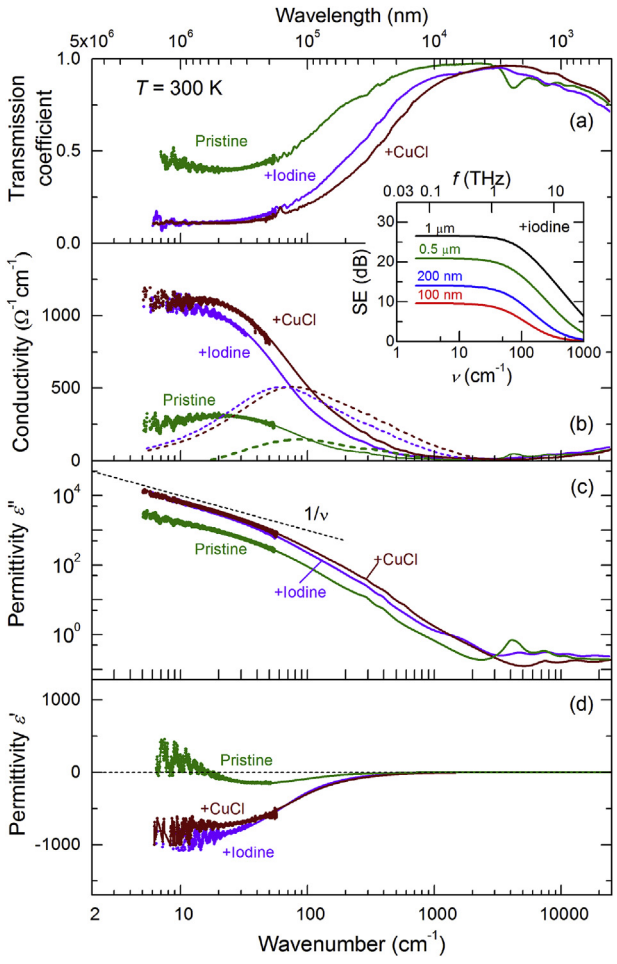


**Fig. 3.** Room temperature spectra of transmission coefficient (a) at terahertz (dots) and infrared (lines) frequencies of three SWCNT films, pristine, CuCl- and iodine-doped. Infrared spectra of real (solid lines in panel b) and imaginary (dashed lines) parts of the conductivity and imaginary (c) and real (d) parts of the permittivity were obtained by spectral analysis of the transmission coefficient spectra, as described in the text. Dots in panels (b, c, d) correspond to the directly measured THz values of conductivity and permittivity. Straight dashed line in panel (c) indicated metallic dependence of the imaginary part of the dielectric permittivity, expression (2). The inset shows shielding effectiveness $SE = -10\log(Tr)$ ($Tr$ – transmission coefficient) for the iodine-doped film calculated for different thickness using the measured spectra of conductivity and permittivity. (A colour version of this figure can be viewed online.)

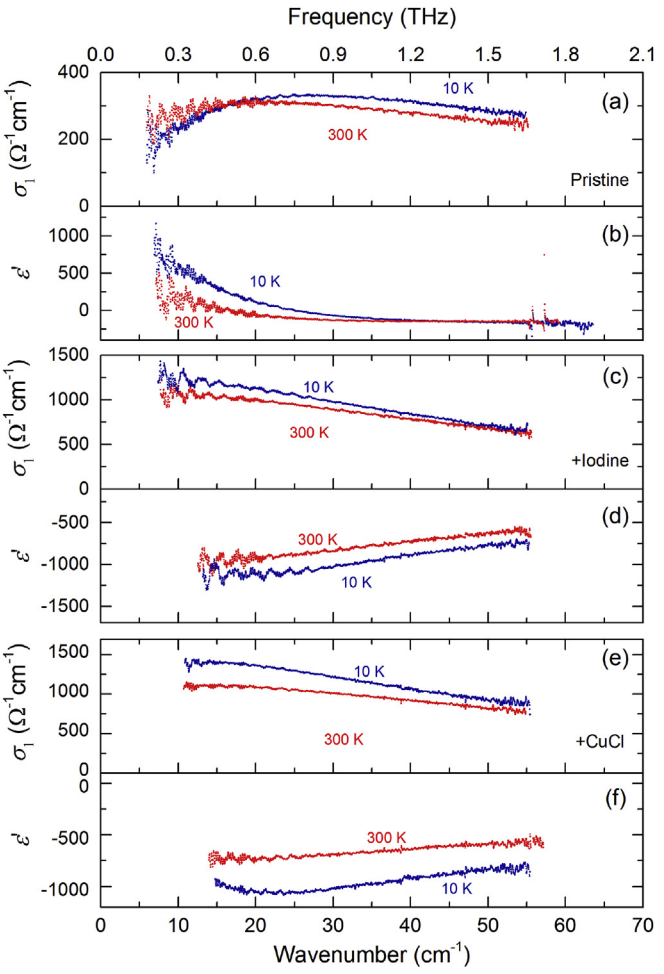


**Fig. 4.** Terahertz spectra of conductivity (a, c, e) and real permittivity (b, d, f) of pristine, CuCl- and iodine-doped SWCNT films, measured at room temperature and at 10 K. (A colour version of this figure can be viewed online.)

pristine films, along with the overall metallic character of the frequency-temperature dependences of their conductivity and permittivity at frequencies above ≈40 $cm^{-1}$, some deviations are observed at lower frequencies where additional factors start to play role in the dynamics of the charge carriers condensate as will be discussed later.

Having known that the terahertz spectral response of the studied SWCNT films is determined by delocalized charge carriers, we can apply Drude Eqs. (1) and (2) to process the measured THz-IR transmission coefficient spectra together with the directly determined THz conductivity and permittivity, in order to obtain the broad-band spectra of conductivity and dielectric permittivity. (The minima in the range 3000 to 25 000 $cm^{-1}$ caused by interband transitions were modeled with Lorentzian lineshapes). The results of the corresponding spectral analysis are shown by lines in Fig. 3b, c, d. Using the formalism of the Drude conductivity model and corresponding expressions (1), (2) we can obtain the temperature dependences of the effective charge carriers parameters: the plasma frequency, the scattering rate, the concentration, the mobility, the mean-free path and the collision time. The results are presented in Fig. 5 and the room temperature values of the parameters are collected in Table 1.

Obviously, all these values are effective and characterize the random network of large amount of nanotubes composing the films with the filling factor <100%; in addition, the conductivity and the permittivity spectra are determined not only by an intrinsic response of the SWCNTs, but also by the inter-tube contacts. This means that the obtained parameters' values are underestimated when compared to the quantities characterizing individual SWCNTs whose mobility (of order of tens of thousands of $cm^2V^{-1}s^{-1}$ [35]) and mean-free paths (of order of micrometers [36]) are much higher. Nevertheless, the obtained numbers of the charge carriers' parameters and their temperature dependences are physically meaningful and agree with the data on the SWCNT films available in the literature. We note that although the effective scattering rate of the CuCl-doped film is larger than that of the iodine-doped film, both its conductivity and plasma frequency still exceed those of the iodine-doped film due to larger carrier concentration.

As expected, the conductivity and the plasma frequency of the doped films are considerably larger than these of the pristine film. In accordance with the dc and low-frequency ac experiments (see, for example, [31,39–41]), the THz conductivity of our films first increases while cooling down. It is either saturated (iodine-doped

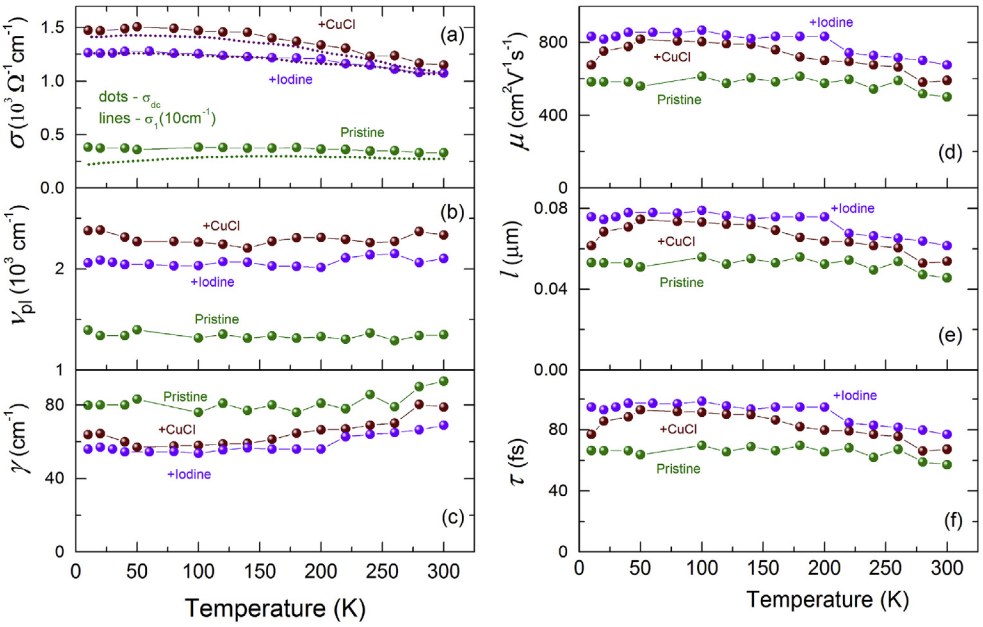


**Fig. 5.** Temperature dependencies of effective parameters of charge carriers of pristine, CuCl- and iodine-doped SWCNT films determined by fitting the THz-IR spectra within the framework of the Drude conductivity model as described in the text. (a). Dc conductivity $\sigma_{dc}$ (dots) determined by fitting the spectra with the Drude expressions (1,2) and conductivity at a frequency of 10 $cm^{-1}$ (dashed lines). (b). Plasma frequency. (c). Scattering rate. (d). Mobility. (e). Mean-free path. (f). Collision time. For the calculations the Fermi velocity was taken as $v_F = 8\times10^7$ cm $s^{-1}$ [37]) and the effective mass as $m^* = 0.2$ $m_e$ [38], where $m_e$ is the free electron mass. (A colour version of this figure can be viewed online.)

**Table 1**
Effective room temperature parameters of charge carriers in pristine, CuCl- and iodine-doped SWCNT films determined on the basis of the Drude model (Eqs. (1) and (2)) description of conductivity and permittivity spectra: plasma frequency $\nu_{pl}$, dc conductivity $\sigma_{dc}$, concentration $n$, scattering rate $\gamma$, mobility $\mu$, collision time $\tau$ and mean-free path $l = v_F\tau$ (with the Fermi velocity $v_F = 8\cdot10^7$ cm $s^{-1}$ [37]). For the calculations the effective mass of the charge carriers were taken as $m^* = 0.2$ $m_e$ [38], where $m_e$ is the free electron mass.

| | Pristine | + iodine | + CuCl |
|---|---|---|---|
| $\nu_{pl}$ ($cm^{-1}$) | 1350 | 2100 | 2340 |
| $\sigma_{dc}$ ($\Omega^{-1}cm^{-1}$) | 330 | 1070 | 1150 |
| $n$ ($cm^{-3}$) | $4\cdot10^{18}$ | $9.9\cdot10^{18}$ | $1.2\cdot10^{19}$ |
| $\gamma$ ($cm^{-1}$) | 93 | 70 | 80 |
| $\mu$ ($cm^2V^{-1}s^{-1}$) | 500 | 675 | 590 |
| $l$ (μm) | 0.05 | 0.06 | 0.05 |
| $\tau$ (fs) | 57 | 77 | 67 |

sample) or slightly decreases below 150–200 K (pristine and CuCl-doped samples). Since the plasma frequency of all samples is basically temperature independent (Fig. 5b), such behavior should be associated with the temperature variation of the scattering rate and, correspondingly, of the mobility, mean-free path and collision time (Fig. 5 c,d,e,f). By analogy with the analysis of the dc resistivity experiments made in Refs. [30,41], we suggest that the mechanism of the observed THz-IR absorption is determined by two contributions to the dc/ac conductivity. The first contribution is connected with the "intrinsic" conductivity of a separate SWCNTs or SWCNT bundles, growing under cooling due to suppression of the phonon scattering process. The second contribution is governed by the fluctuation-assisted tunneling (FAT) of charge carriers through the energy barriers at the inter-tube contacts [42] that becomes less effective at low temperatures. The total static resistivity and conductivity are then expressed as [43,44].

$$R_{dc}(T) = \sigma_{dc}^{-1}(T) = Aexp\left(-\frac{T_m}{T}\right) + B\exp\left(\frac{T_t}{T_s + T}\right). \quad (3)$$

Here, $T_m$ accounts for the backscattering of the charge carriers within the SWCNT (SWCNT bundle), $k_BT_t$ corresponds to the typical energy barrier for the carrier tunneling, the ratio $T_t/T_s$ determines the tunneling in the absence of fluctuations, $A$ and $B$ are temperature independent factors ($k_B$ is the Boltzmann constant). Utilizing this expression allowed to reproduce perfectly the temperature dependence of the dc resistivity of pristine and doped SWCNT films [30] and to estimate the relative values of the SWCNT and the FAT contributions. It was also shown that the high-temperature resistivity is mainly determined by the first term in (3), while the tunneling mechanism becomes dominant below 100–150 K for pristine films and below ≈50 K for doped films. Unlike the dc data, the present temperature dependences of the THz conductivity of the pristine and of the doped films are qualitatively different. This is demonstrated by Fig. 6a. Similarly to the dc conductivity, the THz conductivity of pristine film reveals broad maximum centered around 150–200 K whereas the $\sigma_1$(T) dependences of doped films show monotonous increase towards low temperatures. The distinction is further illustrated by the temperature variations of the normalized THz resistivities of the doped films, Fig. 6 b,c,d, that do not show any low-temperature upturn seen in the dc case. These observations can be understood by taking into account the tunnel barriers or the tunnel energy gaps that are, according to the FAT model, experienced by delocalized charge carriers when they attempt to cross the inter-tube contacts. The values of the gaps are estimated as 1.4–1.6 meV (corresponding to the temperatures $T_t$ = 16–18 K [30]) for pristine SWCNT films and as 0.2–0.25 meV ($T_t$ = 2–3 K [30]) for doped films where smaller gap values can be caused by changes of the work function during doping [45]. When studying the ac response of such carriers, their measured parameters' values and temperature dependences will be different depending on whether the quantum energy $h\nu$ of the probing electromagnetic radiation is smaller or larger than the tunnel gap ($h$ is the Planck's constant). For $h\nu \ll k_BT_t$ the ac and the dc conductivities will have close values and will have similar temperature dependence (if there are no other low-energy processes

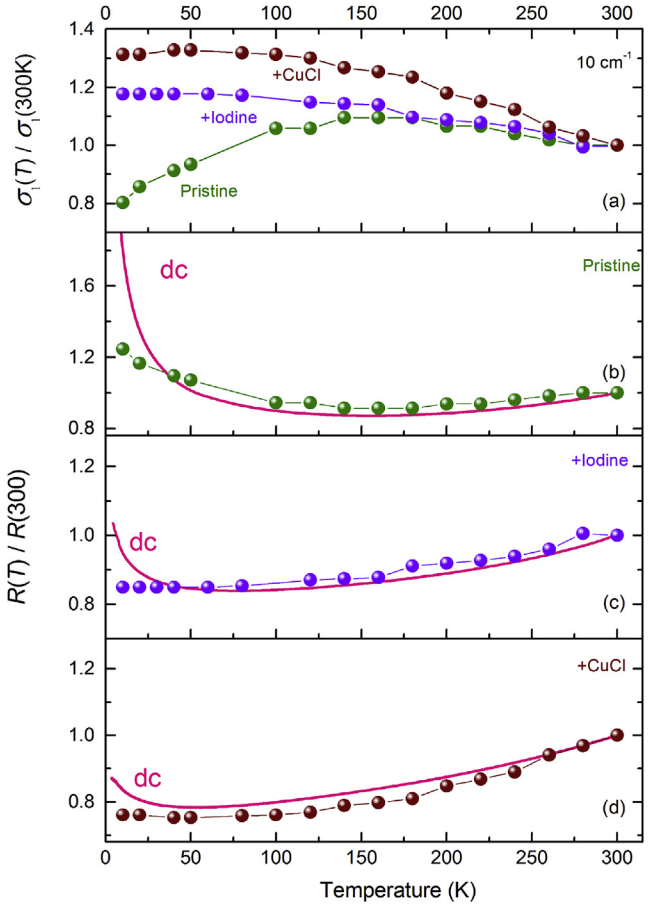


**Fig. 6.** Temperature dependences of normalized conductivities (a) and resistances (b, c, d) of pristine, CuCl- and iodine-doped SWCNT films. Lines show the data from Ref. [30]. (A colour version of this figure can be viewed online.)

involved). At high frequencies, $h\nu \gg k_B T_t$, the probing radiation will not "feel" the presence of the small gap or the shallow energy relief, and the charge carriers will respond to the ac field as if they are free. For example, this kind of optical response is revealed by superconductors where the energy gap in the density of states strongly influences the spectral response only at energies comparable or smaller than the superconducting gap value; at much higher energies the response is indistinguishable from that of a simple metal [46]. Similarly, no signs of the tunnel gaps of 0.2–0.25 meV (corresponding frequencies are 1.4–2 $cm^{-1}$) are detected in our spectra of doped SWCNT films that are measured at significantly higher energies/frequencies, see Figs. 3 and 4.

In case of pristine film, however, the tunnel gap is large (1.4–1.6 meV) and the corresponding frequencies (11-13 $cm^{-1}$) fall in the range where the measurements have been done. This leads to a pronounced decrease at low temperatures of the ac conductivity $\sigma_1(10\ cm^{-1})$, or to the growth of the normalized resistance (Fig. 6 a,b) since now the quantum energy of the radiation is not sufficient to assist effective transition of the carrier over the potential barrier; according to the Kramers-Kronig relations, decrease of $\sigma_1(10\ cm^{-1})$ causes upturn in the lowest frequency permittivity $\varepsilon'(\nu)$, Fig. 5d.

Finally, we comment on the published observations of the terahertz conductivity peak that was detected at frequencies ranging from ≈0.4 THz [47] to ≈30 THz [8] but is not seen in our experiments. We believe that the most likely reason for the absence of the peak in the THz spectra of our SWCNT films is their high quality. The SWCNTs are long (10–20 μm) and the potential barriers impeding charge transport at the tube-tube contacts are rather low, especially in the doped samples (0.2–0.25 meV only). This means that our films can be considered as a network of SWCNTs with the charge carriers being able to relatively easily overcome the barriers at the intersections. This is in accord with our Kelvin-probe characterization of the films demonstrating almost uniform electrical potential over large arrays of the tubes, not significantly influenced

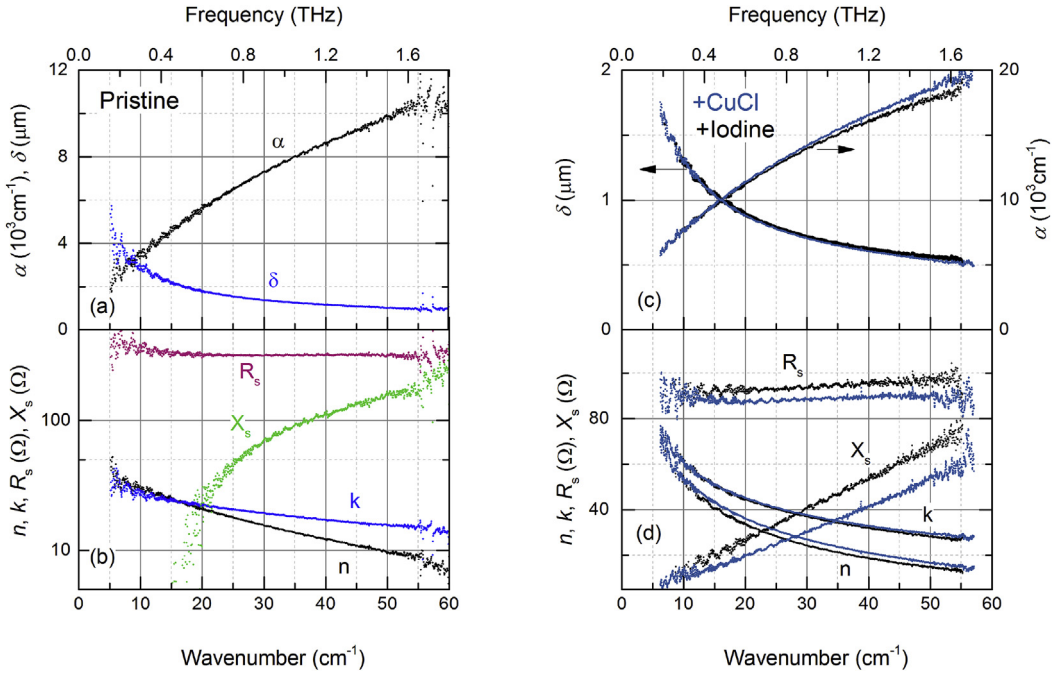


**Fig. 7.** Room temperature spectra of electrodynamic parameters that characterize pristine and doped SWCNT films: absorption coefficient $\alpha = 4\pi k/\lambda$ ($\lambda$ is the radiation wavelength), skin depth $\delta = \lambda(4\pi k)^{-1}$, real n and imaginary $k$ parts of the complex refractive index $n^* = n + ik$, real $R_s$ and imaginary $X_s$ parts of surface resistance $R_S = \sigma_1(\sigma_1^2 + \sigma_2^2)^{-1}$, $X_S = \sigma_2(\sigma_1^2 + \sigma_2^2)^{-1}$. (A colour version of this figure can be viewed online.)

by inter-tube contacts (Fig. 1). For the pristine SWCNTs, however, the tunnel barriers are larger and this leads to partial localization of the carriers and to the appearance of weak peak-like features in the spectra (Fig. 3b).

To our knowledge, this is the first firm experimental evidence for a metallic electromagnetic response of a macroscale SWCNT films in an extremely broad frequency range, basically starting with the dc limit up to the "fundamental" boundary given by the effective scattering rate of the charge carriers within the films. This is realized due to a high chemical and physical quality of separate SWCNTs and a low electrical resistance at inter-tube intersections. Our results demonstrate great opportunities for using SWCNT macrofilms in various microwave and higher-frequency devices like electromagnetic shields, conductive coatings, antennas, filters, resonators, etc. As an example, we show in the inset of Fig. 3 the frequency dependences of the electromagnetic shielding effectiveness, $SE = -10\log(Tr)$ where Tr is the transmission coefficient. The dependences are calculated for different thicknesses of the iodine-doped film using the measured spectra of its conductivity and permittivity. When compared to other materials, like metals, polymers or ceramics, the SWCNT films have significant advantages due to their light weight, chemical and mechanical stability, flexibility and high adhesion to substrates. We note that similar performance at THz frequencies is demonstrated by multi-layer graphene structures [48,49]. However, the advantage of macroscale CNT films is that they are mechanically firmer and can thus be easier handled in their free-standing form. In Fig. 7 we present room temperature spectra of some additional electromagnetic characteristics of the studied three films that can be considered for assessing possibilities of their use in various applications.

In conclusion, the measured terahertz-infrared spectra of optical conductivity and dielectric permittivity of high-quality pristine and doped SWCNT films demonstrate typical metallic-like frequency and temperature behavior. By using the formalism of the Drude conductivity model we determine the temperature dependences of effective parameters of free charge carriers that characterize the films: plasma frequency, scattering rate, mobility. In pristine films, clear signatures of the tunnel gap are detected that governs the dc and the ac transport at low temperatures (below 100–150 K). We demonstrate that the terahertz-infrared spectroscopy is an effective contactless technique that allows to study microscopic transport mechanisms in carbon nanotube layers.

## Acknowledgements

The work was supported by the Russian Ministry of Education and Science (Program '5top100') (terahertz-infrared spectroscopy), by the Russian Science Foundation (project 15-12-30041) (formation, filling and characterization of single-wall carbon nanotube films) and by the MOPPI project of the Aalto University AEF research program (aerosol synthesis of carbon nanotubes) by Skoltech NGP Program (Skoltech-MIT joint project); part of the experiments we performed using equipment of MIPT Shared Facilities Center and with financial support from the Ministry of Education and Science of the Russian Federation, Grant No. RFMEFI59417X0014 (KPFM samples fabrication). We acknowledge fruitful discussions with Prof. S.Tretiak, Dr. G.Fedorov, Dr. M.Shuba and the assistance of Z.V.Gagkaeva and L.S.Kadyrov in spectroscopic measurements and data processing. The work was carried out with a financial support from the Ministry of Education and Science of the Russian Federation as part of Improve Competitiveness Program of NUST "MISIS", implemented by a governmental decree dated 16th of March 2013, № 211.

## References

[1] Q. Zhang, J.-Q. Huang, W.-Z. Qian, Y.-Y. Zhang, F. Wei, The road for nanomaterials industry: a review of carbon nanotube production, post-treatment, and bulk applications for composites and energy storage, Small 9 (2013) 1237–1265, https://doi.org/10.1002/smll.201203252.
[2] M.F.L. De Volder, S.H. Tawfick, R.H. Baughman, A.J. Hart, Carbon nanotubes: present and future commercial applications, Science 339 (6119) (2013) 535–539, https://doi.org/10.1126/science.1222453.
[3] EYu Kataev, D.M. Itkis, A.V. Fedorov, B.V. Senkovsky, DYu Usachov, N.I. Verbitskiy, et al., Oxygen reduction by lithiated graphene and graphene-based materials, ACS Nano 9 (2015) 320–326, https://doi.org/10.1021/nn5052103.
[4] A.I. Chernov, P.V. Fedotov, A.V. Talyzin, I.V. Anoshkin, A.G. Nasibulin, E.I. Kauppinen, E.D. Obraztsova, Optical properties of graphene nanoribbons encapsulated in single-walled carbon nanotubes, ACS Nano 7 (2013) 6346–6353, https://doi.org/10.1021/nn4024152.
[5] Carbon Nanotubes: Synthesis, Structure, Properties, and Applications. In: Dresselhaus MS, Dresselhaus G, editors., Phaedon Avouris. Berlin, Heidelberg, New York:Springer-Verlag; 2001
[6] R.H. Baughman, A.A. Zakhidov, W.A. De Heer, Carbon nanotubes–the route toward applications, Science 297 (5582) (2002) 787–792, https://doi.org/10.1126/science.1060928.
[7] A.G. Nasibulin, A. Kaskela, K. Mustonen, A.S. Anisimov, V. Ruiz, S. Kivistö, et al., Multifunctional freestanding single-walled carbon nanotube films, ACS Nano 5 (2014) 3214–3221, https://doi.org/10.1021/nn200338r.
[8] M.V. Shuba, A.G. Paddubskaya, A.O. Plyushch, P.P. Kuzhir, G.Ya Slepyan, S.A. Maksimenko, et al., Experimental evidence of localized plasmon resonance in composite materials containing single-wall carbon nanotubes, Phys. Rev. B 85 (2012), 165435, https://doi.org/10.1103/PhysRevB.85.165435.
[9] Tae-In Jon, Keun-Ju Kim, Chul Kang, In Hee Maeng, Joo-Hiuk Son, Kay Hyeok An, et al., Optical and electrical properties of preferentially anisotropic single-walled carbonnanotube films in terahertz region, J. Appl. Phys. 95 (10) (2004) 5736–5740, https://doi.org/10.1063/1.1699498.
[10] A. Pekker, K. Kamaras, Wide-range optical studies on various single-walled carbon nanotubes: origin of the low-energy gap, Phys. Rev. B 84 (2011) 075475, https://doi.org/10.1103/PhysRevB.84.075475.
[11] M.E. Itkis, S. Niyogi, M.E. Meng, M.A. Hamon, H. Hu, R.C. Haddon, Spectroscopic study of the fermi level electronic structure of single-walled carbon nanotubes, Nano Lett. 2 (2) (2002) 155–159, https://doi.org/10.1021/nl0156639.
[12] F. Borondics, K. Kamarás, M. Nikolou, D.B. Tanner, Z.H. Chen, A.G. Rinzler, Charge dynamics in transparent single-walled carbon nanotube films from optical transmission measurements, Phys. Rev. B 74 (2006) 045431, https://doi.org/10.1103/PhysRevB.74.045431.
[13] A. Ugawa, A.G. Rinzler, D.B. Tanner, Far-infrared gaps in single-wall carbon nanotubes, Phys. Rev. B 60 (16) (1999) R11305–R11308, https://doi.org/10.1103/PhysRevB.60.R11305.
[14] B. Ruzicka, L. Degiorgi, R. Gaal, L. Thien-Nga, R. Bacsa, J.-P. Salvetat, L. Forro, Optical and dc conductivity study of potassium-doped single-walled carbon nanotube films, Phys. Rev. B 61 (4) (2000) R2468–R2471, https://doi.org/10.1103/PhysRevB.61.R2468.
[15] T. Nakanishi, T. Ando, Optical response of finite-length carbon nanotubes, J. Phys. Soc. Jpn. 78 (11) (2009), 114708, https://doi.org/10.1143/jpsj.78.114708.
[16] T. Morimoto, T. Okazaki, Optical resonance in far-infrared spectra of multi-walled carbon nanotubes, Appl. Phys. Express 8 (2015), 055101, https://doi.org/10.7567/APEX.8.055101.
[17] N. Akima, Y. Iwasa, S. Brown, A.M. Barbour, J. Cao, J.L. Musfeldt, et al., Strong anisotropy in the far-infrared absorption spectra of stretch-aligned single-walled carbon nanotubes, Adv. Mater. 18 (2006) 1166–1169, https://doi.org/10.1002/adma.200502505.
[18] Q. Zhang, E.H. Haroz, Z. Jin, L. Ren, X. Wang, R.S. Arvidson, et al., Plasmonic nature of the terahertz conductivity peak in single-wall carbon nanotubes, Nano Lett. 13 (2013) 5991–5996, https://doi.org/10.1021/nl403175g.
[19] T. Morimoto, S.K. Joung, T. Saito, D.N. Futaba, K. Hata, T. Okazaki, Length-dependent plasmon resonance in single-walled carbon nanotubes, ACS Nano 8 (10) (2014) 9897–9904, https://doi.org/10.1021/nn505430s.
[20] A. Moisala, A.G. Nasibulin, D.P. Brown, H. Jiang, Khriachtchev, L, KauppinenEI. Single-walled carbon nanotube synthesis using ferrocene and iron pentacarbonyl in a laminar flow reactor, Chem. Eng. Sci. 61 (13) (2006) 4393–4402, https://doi.org/10.1016/j.ces.2006.02.020.
[21] Y. Tian, M. Timmermans, S. Kivistö, A.G. Nasibulin, Z. Zhu, H. Jiang, et al., EI. Tailoring the diameters of single-walled carbon nanotubes for optical applications, Nano Res. 4 (8) (2011) 807–815, https://doi.org/10.1007/s12274-011-0137-6.
[22] A. Kaskela, A.G. Nasibulin, M.Y. Timmermans, B. Aitchison, A. Papadimitratos, Y. Tian, et al., Aerosol-synthesized SWCNT networks with tunable conductivity and transparency by a dry transfer technique, Nano Lett. 10 (2010) 4349–4355, https://doi.org/10.1021/nl101680s.
[23] A.A. Tonkikh, V.I. Tsebro, E.A. Obraztsova, K. Suenaga, H. Kataura, A.G. Nasibulin, et al., Metallization of single-wall carbon nanotube thin films induced by gas phase iodination, Carbon 94 (2015) 768–774, https://doi.org/10.1016/j.carbon.2015.07.062.

[24] A.A. Tonkikh, E.D. Obraztsova, E.A. Obraztsova, A.V. Belkin, A.S. Pozharov, Optical spectroscopy of iodine-doped single-wall carbon nanotubes of different diameter, Phys. Status Solidi (b) 249 (2012) 2454–2459, https://doi.org/10.1002/pssb.201200153.
[25] P.V. Fedotov, A.A. Tonkikh, E.A. Obraztsova, A.G. Nasibulin, E.I. Kauppinen, A.L. Chuvilin, et al., Optical properties of single-walled carbon nanotubes filled with CuCl by gas-phase technique, Phys. Status Solidi (b) 251 (2014) 2466–2470, https://doi.org/10.1002/pssb.201451240.
[26] R. Saito, G. Dresselhaus, M.S. Dresselhaus, Trigonal warping effect of carbon nanotubes, Phys. Rev. B 61 (2000) 2981, https://doi.org/10.1103/PhysRevB.61.2981.
[27] R.B. Weisman, S.M. Bachilo, Dependence of optical transition energies on structure for single-walled carbon nanotubes in aqueous suspension: an empirical kataura plot, Nano Lett. 2003 (3) (2003) 1235–1238, https://doi.org/10.1021/nl034428i.
[28] Y. Tian, H. Jiang, J. Pfaler, Zh Zhu, A.G. Nasibulin, T. Nikitin, et al., Analysis of the size distribution of single-walled carbon nanotubes using optical absorption spectroscopy, J. Phys. Chem. Lett. 1 (2010) 1143–1148, https://doi.org/10.1021/jz100161p.
[29] B. Gorshunov, A. Volkov, I. Spektor, A. Prokhorov, A. Mukhin, M. Dressel, et al., Terahertz bwo-spectroscopy, Int. J. Infrared Millim. Waves 26 (2005) 1217–1240, https://doi.org/10.1007/s10762-005-7600-y.
[30] V.I. Tsebro, A.A. Tonkikh, D.V. Rybkovskiy, E.A. Obraztsova, E.I. Kauppinen, E.D. Obraztsova, Phonon contribution to electrical resistance of acceptor-doped single-wall carbon nanotubes assembled into transparent films, Phys. Rev. B 94 (2016), 245438, https://doi.org/10.1103/PhysRevB.94.245438.
[31] O. Hilt, H.B. Brom, M. Ahlskog, Localized and delocalized charge transport in single-wall carbon-nanotube mats, Phys. Rev. B 61 (8) (1999), R5129, https://doi.org/10.1103/PhysRevB.61.R5129.
[32] H. Xu, S.M. Anlage, L. Hu, G. Gruner, Microwave shielding of transparent and conducting single-walled carbon nanotube films, Appl. Phys. Lett. 90 (2007), 183119, https://doi.org/10.1063/1.2734897.
[33] A.V. Sokolov, Optical Properties of Metals, American Elsevier, New York, 1967.
[34] M. Dressel, G. Gruner, Electrodynamics of Solids, Cambridge University Press, Cambridge, 2002.
[35] M. Bockrath, J. Hone, A. Zettl, P.L. McEuen, A.G. Rinzler, R.E. Smalley, Chemical doping of individual semiconducting carbon-nanotube ropes, Phys. Rev. B 61 (2000), R10606, https://doi.org/10.1103/PhysRevB.61.R10606.
[36] J.-Y. Park, S. Rosenblatt, Y. Yaish, V. Sazonova, H. Üstünel, S. Braig, et al., Electron-phonon scattering in metallic single-walled carbon nanotubes, Nano Lett. 3 (3) (2004) 517–520, https://doi.org/10.1021/nl035258c.
[37] L.C. Venema, J.W.G. Wildöer, J.W. Janssen, S.J. Tans, H.L.J. Temminck Tuinstra, L.P. Kouwenhoven, C. Dekker, Imaging electron wave functions of quantized energy levels in carbon nanotubes, Science 283 (1999) 52–55, https://doi.org/10.1126/science.283.5398.52.
[38] J.M. Marulanda, A. Srivastava, Carrier density and effective mass calculations in carbon nanotubes, Phys. Stat. Sol. (b) 245 (11) (2008) 2558–2562, https://doi.org/10.1002/pssb.200844259.
[39] J. Hone, M.C. Llaguno, N.M. Nemes, A.T. Johnson, J.E. Fischer, D.A. Walters, Electrical and thermal transport properties of magnetically aligned single wall carbon nanotube films, Appl. Phys. Lett. 77 (5) (2000) 666–668, https://doi.org/10.1063/1.127079.
[40] T. Takano, T. Takenobu, Y. Iwasa, Enhancement of carrier hopping by doping in single walled carbon nanotube films, J. Phys. Soc. Jpn. 77 (12) (2008), 124709, https://doi.org/10.1143/jpsj.77.124709.
[41] E. Bekyarova, M.E. Itkis, N. Cabrera, B. Zhao, A. Yu, J. Gao, et al., Electronic properties of single-walled carbon nanotube networks, J. Am. Chem. Soc. 127 (2005) 5990–5995, https://doi.org/10.1021/ja043153l.
[42] P. Sheng, Fluctuation-induced tunneling conduction in disordered materials, Phys. Rev. B 21 (1980) 2180, https://doi.org/10.1103/PhysRevB.21.2180.
[43] A.B. Kaiser, G. Dusberg, S. Roth, Heterogeneous model for conduction in carbon nanotubes, Phys. Rev. B 57 (1998) 1418, https://doi.org/10.1103/PhysRevB.57.1418.
[44] A.B. Kaiser, Electronic transport properties of conducting polymers and carbon nanotubes, Rep. Prog. Phys. 64 (2001) 1, https://doi.org/10.1088/0034-4885/64/1/201.
[45] K.K. Kim, J.J. Bae, H.K. Park, S.M. Kim, Park KA. Geng H-Zh, et al., Fermi level engineering of single-walled carbon nanotubes by $AuCl_3$ doping, J. Am. Chem. Soc. 130 (38) (2008) 12757–12761, https://doi.org/10.1021/ja8038689.
[46] M. Tinkham, Introduction to Superconductivity, second ed., McGraw-Hill, New York, 1996.
[47] T.-I. Jeon, K.-J. Kim, C. Kang, I.H. Maeng, J.-H. Son, K.H. An, et al., Optical and electrical properties of preferentially anisotropic single-walled carbon nanotube films in terahertz region, J. Appl. Phys. 95 (10) (2004) 5736–5740, https://doi.org/10.1063/1.1699498.
[48] T. Low, P. Avouris, Graphene plasmonics for terahertz to mid-infrared applications, ACS nano 8 (2) (2014) 1086–1101, https://doi.org/10.1021/nn406627u.
[49] K. Batrakov, P. Kuzhir, S. Maksimenko, N. Volynets, S. Voronovich, A. Paddubskaya, et al., Enhanced microwave-to-terahertz absorption in graphene, Appl. Phys. Lett. 108 (12) (2016), 123101, https://doi.org/10.1063/1.4944531.